Proceedings of the 21st ICSMGE, Vienna, Austria, 14 – 19 June 2026. Pistrol, Adam & Schweiger (eds.)
Published by: ÖGG, Austrian Society for Geomechanics, Salzburg, Austria, ISBN 978-3-9503898-4-5
https://doi.org/10.53243/ICSMGE2026-897

Load redistribution in anchored structures due to anchor failure

Matthias J. Rebhan, Hans-Peter Daxer, Johannes Leo, Franz Tschuchnigg
Institute of Soil Mechanics, Foundation Engineering and Computational Geotechnics, Graz University of Technology, Graz, Austria, rebhan@tugraz

ABSTRACT: The structural safety of anchored retaining walls can be significantly compromised by the failure of individual anchors, leading to complex load redistribution effects. Within the framework of the SaRAS research project, medium-scale model tests and field-scale three-dimensional numerical analyses were conducted to investigate these mechanisms under controlled failure scenarios. The findings supported the development of a simplified assessment workflow for practical application in geotechnical engineering. The proposed workflow integrates three components: (1) geotechnical stability analyses in accordance with Eurocode 7; (2) concrete structural modelling in accordance with Eurocode 2; and (3) verification of anchor load-bearing capacity in accordance with Eurocode 3. In geotechnical analyses, overall stability is assessed for both intact and post-failure conditions, using conservative assumptions to represent anchor loss. Concrete structural investigations model the wall as a horizontally rotated, point-supported slab to evaluate bending moments and support reactions under worst-case load conditions. Finally, anchor capacities are verified against tensile strength limits. This approach enables engineers to identify critical failure scenarios and decide whether more advanced analyses are necessary, thereby bridging the gap between detailed numerical simulations and routine condition assessments.

KEYWORDS: Ground anchor, anchored structure, condition assessment, anchor failure, load redistribution, structural safety.

1 INTRODUCTION

In alpine regions such as Austria, anchored retaining structures offer a reliable and cost-effective solution for stabilising deep cuts along infrastructure corridors. As such, they play a key role in ensuring the accessibility and long-term safety of roads and railway networks. To guarantee their reliability – including durability, serviceability, and load-bearing capacity – over service lives of up to 100 years, regular inspections are conducted in accordance with the Austrian RVS guidelines (FSV, 2022). These inspections frequently reveal corrosion-related damage to pre-stressed grouted anchors, which can lead to the failure of individual elements. Therefore, assessing the implications of such damage or failure on overall structural behaviour is essential for maintaining safety.

Although Eurocode 7 (CEN/TC 250, 2013) requires the evaluation of potential consequences arising from the *"failure of a structural element such as a wall, anchor, wale or strut or failure of the connection between such elements"*, this is rarely addressed in routine geotechnical design. This is partly due to the complex, three-dimensional redistribution of stresses that occurs following anchor failure, affecting both the retaining structure and the surrounding soil. However, full three-dimensional analyses are often considered too resource-intensive for standard engineering practice. Moreover, no comprehensive guidelines or regulations currently exist to support the assessment of defective anchors or to quantify their impact on overall structural performance.

Over the past four years, the research project *"Safety and Risk of Anchored Structures"* (SaRAS) has focused intensively on evaluating the structural condition and performance of anchored structures. As part of this work, this paper presents results from medium-scale model tests investigating load redistribution following anchor failure – an area with scarce experimental data; notable exceptions include Stille and Broms (1976), Itoh et al. (2016) and Zheng et al. (2021).

Most existing research focuses on numerical analyses of strut failure (e.g., Pong et al., 2012; Zhang et al., 2018; Choosrithong and Schweiger, 2020), while studies addressing ground anchor failure remain limited (e.g., Zhao et al., 2018). To address this gap, three-dimensional finite element analyses were conducted to investigate load redistribution in field-scale anchored structures.

However, due to the resource-intensive nature of such models, a simplified analysis workflow is proposed to account for anchor failure within practical condition assessments. This workflow aims to facilitate its application in routine geotechnical engineering practice.

2 MEDIUM-SCALE MODEL TESTS

As introduced, the redistribution of forces following anchor failure is critical for the stability and safety of anchored structures. To investigate these load redistribution mechanisms, a series of medium-scale model tests were conducted within the SaRAS research project. These controlled experiments simulated anchor failure scenarios to evaluate force redistribution among adjacent anchors.

2.1 *Test setup*

The model tests were conducted in a test box measuring 1.00 m in width, 1.50 m in height, and 3.00 m in length. Within the box, a modular retaining wall was assembled from nine steel plates arranged in a 3 × 3 grid. All elements were rigidly connected both horizontally and vertically with bolts. The wall was backfilled with rounded gravel, with a grain size ranging from 4 to 8 mm.

To simplify construction within the confined space of the test box, anchors were replaced with horizontal bracing units (struts) to simulate the lateral support provided by pre-stressed grouted anchors. These struts, subjected to compressive loads, rest against a horizontal beam installed in front of the retaining wall. Each strut can be individually pre-stressed by applying torque, allowing for various test configurations. During failure simulation, selected struts are released one at a time to replicate anchor failure and observe the system's response. Load cells installed at the contact points between the retaining wall and the struts measured the resulting redistribution of forces. Additionally, displacement transducers were installed to monitor the wall deformation locally. Since the focus remains on force redistribution, their data are excluded from the subsequent analyses.

Figure 1 shows the front view of the retaining wall. The 3 × 3 grid of steel plates is labelled as follows: the vertical axes are labelled A to C from left to right, and the horizontal anchor rows are numbered 1 to 3 from bottom to top, following the construction sequence. Thus, the central anchor, for example, is designated as B2. Further details on the model tests are provided in Daxer et al. (2024) and Schleicher et al. (2025).

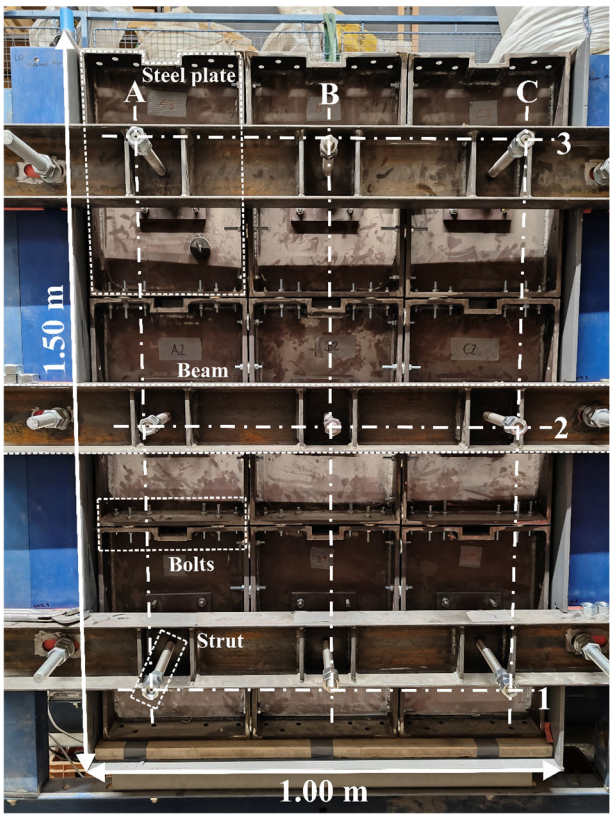

Figure 1. Front view of the test setup to model an anchored retaining wall.

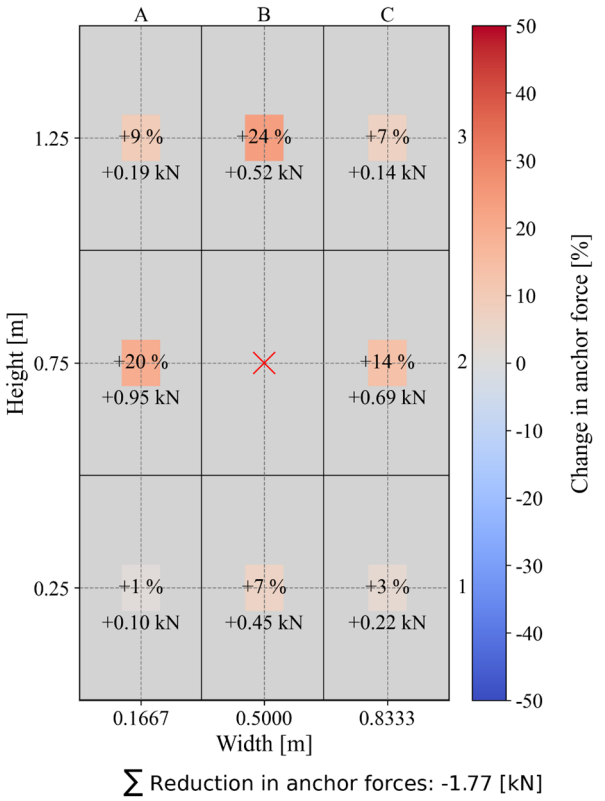

Figure 2. Failure simulation of anchor B2 (adapted from Flatscher, 2025).

2.2 *Results*

Figure 2 shows the results of an anchor failure simulation, conducted by reducing the compressive load in the strut to zero. The figure displays the 3 × 3 grid of steel plates, labelled according to the scheme presented in Figure 1. The failed anchor, B2 in this case, is marked with a red cross. For the remaining anchors, both the absolute and percentage changes in load are shown. Prior to the simulated failure of anchor B2, anchor rows 1, 2 and 3 were pre-stressed to approximately 7 kN, 5 kN, and 2 kN, respectively.

The failure of the central anchor B2 results in an almost symmetrical redistribution of loads. In absolute terms, the largest share of the redistributed load is transferred to the anchors on the left (A2) and right (C2), followed by those directly above (B3) and below (B1) the failed anchor. The largest force increase is observed at anchor A2, which experiences a rise of 0.95 kN (20 %) from its pre-stressing force of 5 kN. Only a relatively small portion of the load is redistributed to the diagonally positioned anchors (A1, C1, A3 and C3).

When considering relative changes, the maximum increase occurs at anchor B3, which rises by 24 % (0.52 kN) from its pre-stressing force of 2 kN. Anchors A2 and C2 also show significant increases of 20 % and 14 %, respectively. For all other anchors, the increase remains below 10 %, and thus they are only of minor importance in this load redistribution scenario.

Summing the absolute force increases in the remaining anchors yields a total of 3.26 kN. This means that 3.26 kN of the 5.03 kN initially carried by anchor B2 prior to the simulated failure are transferred to adjacent anchors. The remaining 1.77 kN are assumed to be redistributed within the soil body or lost due to other effects. This residual value is shown in the lower part of Figure 2. In other words, 65 % of the failed anchor's load is transferred to other anchors.

3 NUMERICAL STUDIES

This chapter presents numerical investigations into the behaviour of field-scale anchored structures subjected to various anchor failure scenarios. To this end, three-dimensional finite element analyses were conducted using PLAXIS 3D (Seequent/Bentley Systems, 2024). The studies primarily focus on the distribution of forces within the pre-stressed ground anchors and their redistribution under different failure conditions. Additionally, internal forces in the retaining wall – such as bending moments – are analysed.

3.1 *Three-dimensional finite element model*

Figure 3 illustrates the three-dimensional finite element mesh with overall dimensions of 140 m (width) × 60 m (height) × 25 m (depth). The initial geometry – prior to the construction of the anchored retaining wall – features a slope inclined at 20° with a height of 14.49 m. The soil mass was modelled as a homogeneous stratum, with no groundwater present in the analyses. For the model discretisation, 298,280 ten-node tetrahedral elements were employed.

In Figure 4, the excavation of the slope in five stages (ES1 to ES5) is shown, progressing from top to bottom. Each excavated soil wedge measures approximately 2.90 m in height and extends over the full model depth of 25 m. At each stage, the removed wedge is replaced by the anchored structure. The retaining wall is inclined 15° from the vertical, with elements anchored centrally – both in height and width – forming five anchor rows (AR1 to AR5). All anchors are inclined 15° from the horizontal (orthogonal to the wall), featuring a free length of 20 m and a bond length of 6 m, yielding a total length of 26 m.

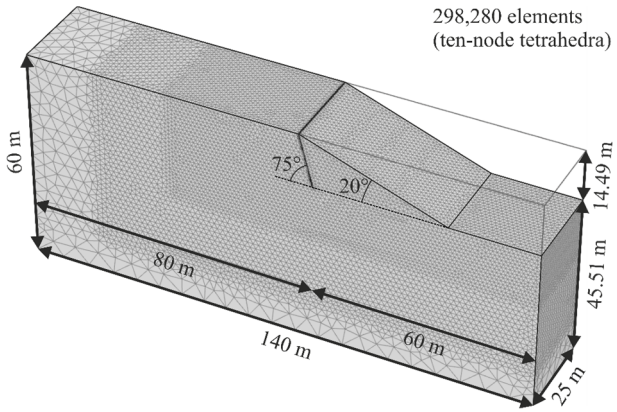

Figure 3. Three-dimensional finite element mesh with dimensions.

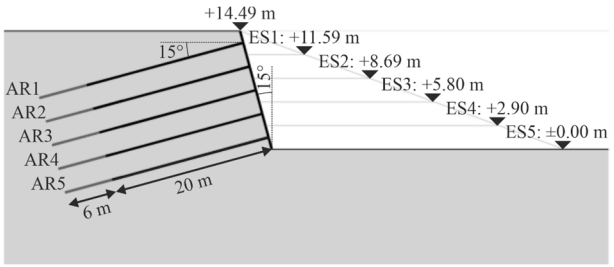

Figure 4. Side view showing the excavation stages and anchor rows.

The front view of the retaining wall is shown in Figure 5. It spans 25 m in width and 15 m in height. Although the wall is inclined at 15° from the vertical in the model, the front view is depicted in a vertical orientation. This rotation allows the true wall height of 15 m to be visualised, rather than the projected height of 14.49 m (*15 m × cos(15°)*). In the three-dimensional model, the 0.60 m thick wall is composed of 25 individual elements, each measuring 5 m in width and 3 m in height, arranged in a 5 × 5 grid. All elements are rigidly connected both horizontally and vertically. As noted above, each element is centrally anchored, resulting in a regular anchor spacing of 5 m horizontally and 3 m vertically. The vertical distance from the top and bottom of the wall to the nearest anchor row is 1.50 m, while the lateral distance to the model's side boundaries is 2.50 m. Horizontal axes are labelled A to E from left to right, and the anchor rows are numbered 1 to 5 vertically from top to bottom (which differs from the labelling convention in Chapter 2). Anchor positions are again identified using grid coordinates, such as C3 for the central anchor.

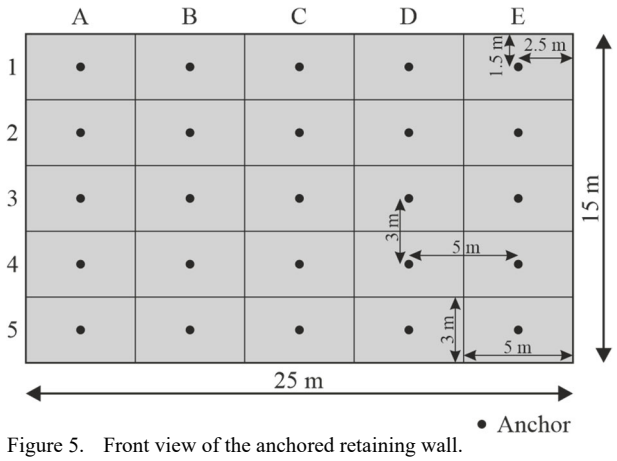

Figure 5. Front view of the anchored retaining wall.

3.2 *Parameters*

To represent soil behaviour as realistically as possible, the homogeneous soil body is modelled using the Hardening Soil model with small-strain stiffness (Schanz, 1998; Benz, 2007). In addition to stress-dependent stiffness and stress-path dependency, the model also accounts for an increased stiffness at very small strains. The corresponding model parameters are listed in Table 1.

Table 1. Soil parameters of the Hardening Soil Small model.

Parameter	Symbol	Value	Unit
Drainage type	-	Drained	-
Unsaturated/Saturated unit weight	γ_{unsat}, γ_{sat}	20	kN/m³
Primary deviatoric modulus	E_{50}^{ref}	$20E^3$	kN/m²
Primary oedometric modulus	E_{oed}^{ref}	$20E^3$	kN/m²
Unloading/Reloading modulus	E_{ur}^{ref}	$60E^3$	kN/m²
Unloading/Reloading Poisson's ratio	ν_{ur}	0.20	-
Power for stress dependency of stiffness moduli	m	0.50	-
Reference pressure for stiffness moduli	p_{ref}	100	kN/m²
Stiffness at very small strains	G_0^{ref}	$75E^3$	kN/m²
Shear strain for which $G_{sec} = 0.7 \times G_0$	$\gamma_{0.7}$	$0.15E^{-3}$	-
Cohesion	c'_{ref}	5	kN/m²
Friction angle	φ'	38	°
Dilatancy angle	ψ	8	°
Coefficient of earth pressure at rest for normally consolidated soils	K_0^{nc}	$1 - \sin \varphi'$	-
Interface strength reduction factor	R_{inter}	0.90	-
Coefficient of earth pressure at rest	K_0	$1 - \sin \varphi'$	-
Overconsolidation ratio	OCR	1	-

The wall is modelled as an elastic plate element. To account for realistic soil-structure interaction, interfaces are defined on the earth-facing side along the entire wall height. The corresponding material parameters are shown in Table 2.

Table 2. Parameters of the wall modelled as plate element.

Parameter	Symbol	Value	Unit
Material type	-	Elastic	-
Unit weight	γ	15	kN/m³
Isotropic	-	Yes	-
Young's modulus	E_1	$30E^6$	kN/m²
Poisson's ratio	ν	0.20	-
Thickness	d	0.60	m
Prevent punching	-	No	-

The pre-stressed ground anchors are modelled using two element types: first, elastoplastic node-to-node anchor elements to represent the free length, and second, elastic embedded beam elements to represent the bond length. The associated parameters are listed in Table 3 (free length) and Table 4 (bond length).

Table 3. Parameters of the tendon modelled as node-to-node anchor.

Parameter	Symbol	Value	Unit
Material type	-	Elastoplastic	-
Axial rigidity	EA	$126E^3$	kN
Tensile strength	$\|F_{max,tens}\|$	856	kN
Compressive strength	$\|F_{max,comp}\|$	0	kN

Table 4. Parameters of the grout body modelled as embedded beam.

Parameter	Symbol	Value	Unit
Material type	-	Elastic	-
Unit weight	γ	4	kN/m³
Diameter (Circular beam)	$Ø$	0.14	m
Young's modulus	E	$16.50E^6$	kN/m²
Axial skin resistance	-	Linear	-
Max. skin friction – start	$T_{skin,start,max}$	700	kN/m
Max. skin friction – end	$T_{skin,start,end}$	700	kN/m
Max. base resistance	F_{max}	0	kN

3.3 *Calculation phases*

The finite element analyses simulate the behaviour of the anchored structure during construction, regular operation and selected anchor failure scenarios.

In Phase 0, the initial stress state is determined. Due to the inclined geometry, this is achieved through gravity loading.

The initial phase is followed by Phase 1, a so-called plastic nil step, which compensates for remaining out-of-balance forces in the model. Subsequently, displacements and small strains are reset to zero to ensure a realistic determination of the deformation behaviour.

Phase 2 involves the first excavation stage, the installation of the associated wall elements including interfaces, and the insertion of the first anchor row.

In Phase 3, each anchor within this row is pre-stressed by 500 kN.

The process of excavation, wall construction including interfaces, anchor installation and pre-stressing of the respective anchor row is repeated for the subsequent levels until, in Phase 11, the fifth anchor row is finally pre-stressed. This last phase corresponds to the regular operational state of the anchored structure.

Following Phase 11, four anchor failure cases are modelled as follows:

- Failure case 1 (FC1): Failure of anchor C3
- Failure case 2 (FC2): Failure of anchors B3, C3 and D3
- Failure case 3 (FC3): Failure of anchors C2, C3 and C4
- Failure case 4 (FC4): Failure of the entire anchor row 3

Anchor failure is simulated by selectively deactivating the affected anchors. Both the tendon (modelled as a node-to-node anchor) and the grout body (modelled as an embedded beam) are deactivated.

3.4 *Results*

Figure 6 illustrates the bending moment distribution following the final construction phase (Phase 11). The anchor forces at each anchor position are also shown. It is evident that the anchor forces increase only slightly beyond their pre-stressing values during the staged construction. Starting from an initial pre-stressing force of 500 kN, the values increase moderately, reaching approximately 512 kN, 524 kN, 536 kN and 531 kN in anchor rows 1 through 4, respectively. Since anchor row 5 is pre-stressed during the final construction phase, its force remains at 500 kN.

As expected, the forces are uniformly distributed within each anchor row prior to the simulated failure cases. As described earlier, the highest anchor forces are observed in anchor row 3 (~536 kN), followed by rows 4, 2 and 1, with row 5 showing the lowest values. Given the tensile strength of 856 kN (see Table 3) for the anchor tendons, this corresponds to a utilization ratio of approximately 63 % for anchor row 3 prior to the simulated failure scenarios. The total anchor force, 13,016 kN, is indicated in the figure's lower right corner.

A maximum moment of approximately -171 kNm/m is oberserved regarding the bending moment distribution.

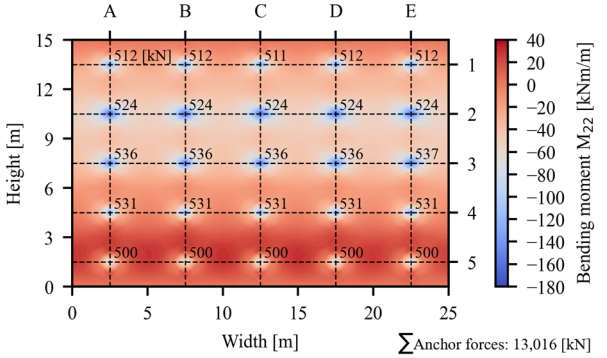

Figure 6. Bending moment distribution after final construction phase.

In Figure 7, the difference in the bending moment distribution between FC1 and the final construction phase is shown. As in the previous figure, the anchors are annotated at each position – now indicating the absolute change in force (kN), with the percentage change (%) shown below. In the failed anchor C3, the force drops by 536 kN (100 %) to zero. This loss leads to a three-dimensional redistribution of anchor forces within the system, which is (as expected) perfectly symmetric both horizontally and vertically in FC1.

The maximum increase, both in absolute and relative terms, occurs in the anchor above the failed element – namely C2. Here, the force increases from 524 kN by 7 kN (1 %) to 532 kN. The highest overall force remains in anchor row 3, specifically in anchor B3, which increases from 536 kN by 5 kN (1 %) to 542 kN.

This moderate increase does not represent a critical load for the pre-stressed ground anchors. Based on the tensile strength, the utilisation ratio remains around 63 % for anchor B3, leaving a reserve of 37 %.

In the lower right corner, the total increase in anchor force in the remaining anchors is compared with the force loss in the failed anchor C3. Numerically, only 70 kN (13 %) of the 536 kN is redistributed to the other anchors; the remaining 466 kN (87 %) is redistributed within the soil body.

Across all failure cases, the highest anchor force is observed in FC4 (failure of the entire anchor row 3), where anchor row 4 reaches 558 kN. This case also marks the largest absolute and percentage increase, rising by 26 kN (5 %) from 531 kN. Even in this conservative (and unrealistic) scenario, the utilisation ratio is around 65 %, confirming adequate safety reserves.

For all simulated failure cases, only a small portion of the lost anchor forces is transferred to the remaining anchors. Depending on the case, approximately 13 % to 17 % of the total anchor force are redistributed to other anchors, while the remaining 87 % to 83 % – summing to 100 % in each case – are redistributed within the soil.

Figure 7 shows that the bending moment near the failed anchor changes significantly – by approximately 196 kNm/m. While this failure case has limited impact on the anchors themselves, the concrete structure must be adequately reinforced to accommodate the resulting force redistribution.

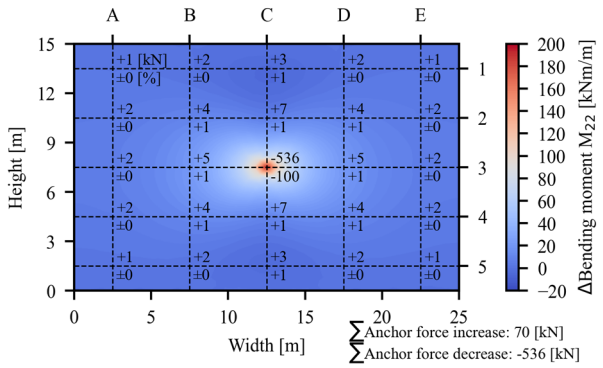

Figure 7. Difference in bending moment distribution between FC1 and the final construction phase.

Figure 8 shows the difference in the bending moment distribution between FC3 and the final construction phase. In this case, however, some of the soil parameters from Table 1 were varied ($E_{50}^{ref} = E_{oed}^{ref} = 17E^3$ kN/m²; $E_{ur}^{ref} = 51E^3$ kN/m²; $G_0^{ref} = 63.75E^3$ kN/m²; $c'_{ref} = 3$ kN/m²; $\varphi' = 30$ °; $\psi = 0$ °).

As a result, anchor row 3 already exhibits anchor forces of approximately 801 kN after the final construction phase, which corresponds to a utilisation ratio of 94 % before simulating anchor failure.

Due to the low safety reserves, the entire anchor row 3 fully plasticises (indicated by the red values in Figure 8). In other words, anchor row 3 reaches its tensile capacity and can no longer accommodate additional load. In a real structure, this would imply structural failure of the affected anchors.

As a result of this plastic behaviour, the load redistribution changes significantly. In this scenario, a larger portion – 1,264 kN (56 %) of the total anchor force loss of 2,272 kN – is redistributed to the remaining anchors, while 1009 kN (44 %) is redistributed within the soil.

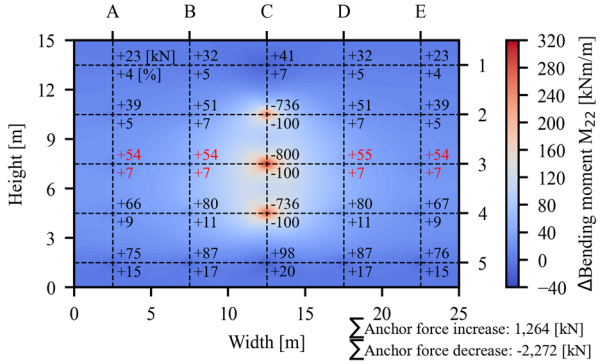

Figure 8. Difference in bending moment distribution between FC3 and the final construction phase for different soil type.

4 SIMPLIFIED ASSESSMENT WORKFLOW

In addition to guidelines developed in collaboration with the SaRAS research project – such as the "RVS Arbeitspapier Nr. 33" (FSV, 2022), which outlines special inspection methods for anchored structures, including endoscopies and lock-off tests – a simplified approach has also been developed to account for anchor failure in condition assessments. This workflow is essentially divided into three parts:

- Geotechnical investigations in accordance with Eurocode 7 (CEN/TC 250, 2013);
- Structural investigation of the concrete elements in accordance with Eurocode 2 (CEN, 2014a);
- Investigation of anchor load-bearing capacity in accordance with Eurocode 3 (CEN, 2014b).

This workflow is described in the following sections, structured according to these components. It aims to account for anchor failure where possible and, where this is not feasible, support the decision-making process regarding the need for more detailed investigations (see Chapter 3).

4.1 *Geotechnical investigations*

From a geotechnical perspective, overall stability – as one of the major failure criteria for anchored structures – is assessed using simplified two-dimensional analytical models, as illustrated in Figure 9. These analyses are conducted for both the intact state (i.e. before anchor failure) and the post-failure condition to quantify such impacts on the factor of safety. However, such models are not capable of simulating the failure of individual anchors. Instead, the deactivation of a single anchor is approximated by removing an entire anchor row, representing a deliberately conservative assumption within the scope of this method.

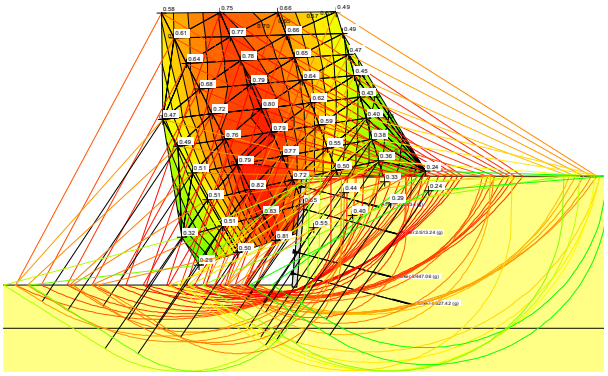

Figure 9. Two-dimensional stability analysis considering anchor failure.

4.2 *Concrete structural investigations*

In the second part of the assessment – the structural analysis – the concrete elements of the anchored wall are idealised by rotating them horizontally and are modelled as a slab supported at discrete points (Figure 10), with each support representing a ground anchor. The redistributed earth pressure is applied as a surface load in accordance with applicable design standards (ON, 1993). This yields an approximation of the bending moment distribution and anchor forces for the intact wall, prior to simulating anchor failure.

Anchor failure is simulated by removing support points according to predefined failure scenarios. The earth pressure remains constant, meaning no redistribution or the deformation related behaviour of it (e.g., Stastny et al., 2025) is considered. Consequently, the entire load must be transferred by the concrete slab to the remaining supports – representing a conservative, worst-case scenario for the structure.

This simplified modelling approach enables efficient evaluation of multiple failure scenarios and allows consideration of various slab connection types, such as rigid joints, shear-dowelled connections, or segmented elements.

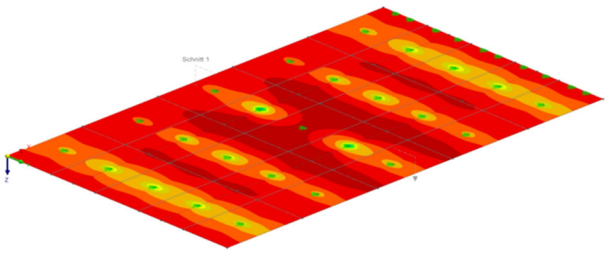

Figure 10. Bending moment distribution of an anchored wall idealised as a slab with discrete point supports.

4.3 *Investigation of anchor load-bearing capacity*

Finally, the anchors (discrete point supports as described in Section 4.2) are assessed for their ability to sustain the additional "generated" loads due to the redistribution. Verification is typically carried out by checking that the tensile capacity is not exceeded, in accordance with the applicable design standards' load-bearing capacity requirements. Additionally, damage symptoms, results of a safety assessment or known weak points of anchor systems (e.g., hydrogen induced stress corrosion cracking) can be included into these investigations.

5 CONCLUSIONS

This study presents an in-depth investigation of load redistribution mechanisms in anchored retaining structures following ground anchor failure, combining medium-scale model tests and three-dimensional field-scale numerical analyses. The model tests demonstrate that approximately 65 % of the failed anchor's load is transferred to adjacent anchors. However, this trend differs notably from the numerical analyses conducted for the investigated soil type, where only about 13 % of the lost anchor load is redistributed to remaining anchors, with the majority being redistributed within the soil. For the second soil type, characterised by different soil strength and stiffness parameters, the numerical results indicate a significantly higher redistribution ratio of around 56%, as the remaining anchors approach their tensile capacity, leading to plastic behaviour.

These discrepancies highlight important differences in load transfer mechanisms that must be considered in design and condition assessment. Limitations in the model tests – particularly the unknown influence of wall friction and the use of simplified bracing units instead of actual ground anchors – may affect the direct comparability with numerical results and real-world conditions.

Overall, the findings underline the necessity for comprehensive assessment workflows that integrate both experimental and numerical approaches to better understand load redistribution after anchor failure. The proposed simplified workflow aims to support practical condition assessments by accounting for anchor failure effects and guiding decision-making for further detailed investigations. Structural safety can be maintained by ensuring that the concrete wall design accommodates increased bending moments resulting from such failures.

6 ACKNOWLEDGEMENTS

The contents in this paper have been developed as part of the research project "Safety and Risk of Anchored Structures" (SaRAS). The authors express their gratitude for the funding provided by the Austrian Research Promotion Agency (FFG).

7 REFERENCES

Benz, T. 2007. *Small-Strain Stiffness of Soils and its Numerical Consequences*. Mitteilung 55 des Instituts für Geotechnik, Dissertation, University of Stuttgart, Stuttgart

CEN/TC 250 2013. *Eurocode 7: Geotechnical design – Part 1: General rules*. EN 1997-1:2004 + AC:2009 + A1:2013, Brussels, Belgium

CEN/TC 250 2014a. *Eurocode 2: Design of concrete structures – Part 1-1: General rules and rules for buildings*. EN 1992-1-1:2004 + AC:2008 + AC:2010 + A1:2014, Brussels, Belgium

CEN/TC 250 2014b. *Eurocode 3: Design of steel structures – Part 1-1: General rules and rules for buildings*. EN 1993-1-1:2005 + AC:2006 + AC:2009 + A1:2014, Brussels, Belgium

Choosrithong, K., and Schweiger, H.F. 2020. Numerical Investigation of Sequential Strut Failure on Performance of Deep Excavations in Soft Soil. *International Journal of Geomechanics* 20(6), 12pp. https://doi.org/10.1061/(ASCE)GM.1943-5622.0001695

Daxer, H.-P., Flatscher, G.O., Tschuchnigg, F., Rebhan, M.J., Pamminger, V., and Wirthl, D. 2024. Simulation and numerical back analysis of the load redistribution associated with degrading anchored structures. *Proceedings of the 5th European Conference on Physical Modelling in Geotechnics*, Delft, 2024, October 2-4, 6pp. https://doi.org/10.53243/ECPMG2024-87

Flatscher, G.O. 2025. *Versuchstechnische Betrachtungen zu Änderungen der Vorspannkraft bei geankerten Konstruktionen*. Master's Thesis, Graz University of Technology, Graz

FSV 2022. *Qualitätssicherung bauliche Erhaltung – Überwachung, Kontrolle und Prüfung von Kunstbauten – Geankerte Konstruktionen*. RVS 13.03.21, Vienna, Austria

FSV 2022. *Sonderprüfmethoden für geankerte Konstruktionen und Zugelemente*. RVS Arbeitspapier Nr. 33, Vienna, Austria

Itoh, K., Kikkawa, N., Toyosawa, Y., Suemasa, N., and Katada, T. 2016. Failure Mechanism of Anchored Retaining Wall Due to the Breakage of Anchor Head. In *Forensic Geotechnical Engineering*, Rao, V.V.S., and Sivakumar Babu, G.L. (eds.), 175-186. PA: Springer India. https://doi.org/10.1007/978-81-322-2377-1_12

ON 1993. *Erd- und Grundbau – Erddruckberechnung*. ÖNORM B 4434, Vienna, Austria

Pong, K.F., Foo, S.L., Chinnaswamy, C.G., Ng, C.C.D., and Chow, W.L. 2012. Design considerations for one-strut failure according to TR26 – a practical approach for practising engineers. *The IES Journal Part A: Civil & Structural Engineering* 5(3), 166-180. https://doi.org/10.1080/19373260.2012.700790

Schanz, T. 1998. *Zur Modellierung des mechanischen Verhaltens von Reibungsmaterialien*. Mitteilung 45 des Instituts für Geotechnik, Habilitation, University of Stuttgart, Stuttgart

Schleicher, J., Rebhan, M.J., Daxer, H.-P., Pamminger, V., Arnold, A., and Tschuchnigg F. 2025 (forthcoming). Tactile Pressure Sensors to analyse Anchor Wall Behaviour in mid-scale Experiments. *Proceedings of the 13th International Conference of Structural Health Monitoring of Intelligent Infrastructure*, Graz, 2025, September 1-5

Seequent/Bentley Systems 2024. *PLAXIS 3D V2024.1.0.1060*

Stastny, A., Emera, A., Galavi, V., and Tschuchnigg, F. 2025. Cyclic soil-structure interaction of intregral railway bridges. *Frontiers in Built Environment* 11, 20pp. https://doi.org/10.3389/fbuil.2025.1541282

Stille, H., and Broms, B.B. 1976. Load redistribution caused by anchor failures in sheet pile walls. *Proceedings of the 6th European Conference on Soil Mechanics and Foundation Engineering*, Vol. 1.2, Vienna, 1976, March 22-24, 197-200.

Zhang, W., Zhang, R., Fu, Y., Goh, A.T.C., and Zhang, F. 2018. 2D and 3D numerical analysis on strut responses due to one-strut failure. *Geomechanics & Engineering* 15(4), 965-972. https://doi.org/10.12989/gae.2018.15.4.965

Zhao, W., Han, J.-Y., Chen, Y., Jia, P.-J., Li, S.-G., Li, Y., and Zhao, Z. 2018. A numerical study on the influence of anchorage failure for a deep excavation retained by anchored pile walls. *Advances in Mechanical Engineering* 10(2), 16pp. https://doi.org/10.1177/1687814018756775

Zheng, G., Lei, Y.W., Cheng, X.S., Li, X.Y., and Wang, R.Z. 2021. Experimental study on progressive collapse mechansim in braced and tied-back retaining systems of deep excavations. *Candadian Geotechnical Journal* 58(4), 540-564. https://doi.org/10.1139/cgj-2019-0296